Orientational dynamics of ferrofluids with finite magnetic anisotropy of the particles: Relaxation of magneto-birefringence in crossed fields

Yu. L. Raikher,[1,2,*] V. I. Stepanov,[1] J.-C. Bacri,[2,†] and R. Perzynski[2]
[1]*Institute of Continuous Media Mechanics, Ural Division of RAS, 1 Korolyov Street, Perm 614013, Russia*
[2]*Laboratoire des Milieux Désordonnés et Hétérogènes, Université Pierre et Marie Curie (Paris 6), Tour 13, Case 78, 4 place Jussieu, 75252 Paris Cedex 05, France*
(Received 25 February 2002; published 14 August 2002)

Dynamic birefringence in a ferrofluid subjected to crossed bias (constant) and probing (pulse or ac) fields is considered, assuming that the nanoparticles have finite magnetic anisotropy. This is done on the basis of the general Fokker-Planck equation that takes into account both internal magnetic and external mechanical degrees of freedom of the particle. We describe the orientation dynamics in terms of the integral relaxation time of the macroscopic orientation order parameter. To account for an arbitrary relation between the bias (external) and anisotropy (internal) fields, an interpolation expression for the integral relaxation time is proposed and justified. A developed description is used to interpret the measurements of birefringence relaxation in magnetic fluids with nanoparticles of high (cobalt ferrite) and low (maghemite) anisotropy. The proposed theory appears to be in full qualitative agreement with all the experimental data available.

DOI: 10.1103/PhysRevE.66.021203 PACS number(s): 75.50.Mm, 78.20.Fm, 05.40.−a, 75.20.−g

I. INTRODUCTION

Dynamic field-induced birefringence is a well-known experimental tool to study magnetic fluids (MFs), see Ref. [1], for example. The majority of the known facts agree with the hypothesis that the ferrite nanoparticles constituting the solid phase of a MF have a slightly anisometric shape. This infers a simple generic mechanism of the field-induced birefringence. The external field orients the particle magnetic moments, and, via them, the particles themselves, thus establishing in a MF an orientational order. Therefore, a system, which (due to the Brownian rotary motion of the particles) was isotropic in the field-free state, acquires a macroscopic uniaxial optical anisotropy. Since the magnetic moments of the particles are much greater than atomic or molecular ones, the resulting birefringence by several orders exceeds the usual Cotton-Mouton effect in liquids and is observed and registered easily.

The description of the orientational mechanism of MF birefringence is based on the orientation-dependent magnetic energy of a single-domain particle subjected to a magnetic field $\boldsymbol{H}=H\boldsymbol{h}$, that is,

$$U=-IV_mH(\boldsymbol{e}\cdot\boldsymbol{h})-E_a(\boldsymbol{e}\cdot\boldsymbol{n})^2, \tag{1}$$

where I is the magnetization of the particle substance and $\boldsymbol{e}$ is the unit vector of the magnetic moment, i.e., $\boldsymbol{\mu}=IV_m\boldsymbol{e}$, where V_m is the volume of the ferromagnetic core of the particle. In highly dispersed systems, like MFs, due to the surface effects V_m is smaller than the total physical volume V of the grain. In Eq. (1) $E_a>0$ is the energy of uniaxial magnetic anisotropy, and $\boldsymbol{n}$ the unit vector of the easy axis. There exist at least three well-proven sources of E_a: volumetric crystallographic, shape, and surface anisotropies. For a dilute MF in equilibrium, an exhaustive description of the macroscopic properties, including the orientational-optical ones, is achieved by substituting the energy (1) in the Gibbs distribution function.

In a dynamic situation the induced orientational order (and, consequently, birefringence) of a MF evolves with the response time(s) of the particles. The appropriate theoretical approach was developed in Ref. [2]. On equal basis it takes into account the effects of both internal (magnetic) and external (mechanical) orientational relaxations of the particles on the birefringence in a MF. Besides uniting several former approximate models of Refs. [3–5], the new theory covers a variety of intermediate cases formerly unaccessible. The particular problem considered in Ref. [2] was the birefringence induced in a MF by a linearly polarized weak ac field. In the present study we extend the theory to the case of a MF subjected to a combination of mutually perpendicular constant (bias) and pulse or ac (probing) magnetic fields. This configuration has been recently realized experimentally and tested for both highly anisotropic and low-anisotropic ferrites in a wide range of bias-field strengths [6]. On the basis of the developed theory we analyze the obtained field strength and frequency dependencies of the dynamic birefringence.

The paper is organized as follows. Section I presents some reasoning on the problem and introduces the general Fokker-Plank equation that accounts for the joint orientational motion of the mechanical and magnetic degrees of freedom of a particle with finite magnetic rigidity. In Sec. II an account on birefringence in a MF of magnetically hard (infinitely rigid) nanoparticles is given and the concept of the integral relaxation time is introduced. Section III is the main theoretical one. There the dynamic birefringence in a MF with particles of finite magnetic anisotropy is described in terms of a single (integral) relaxation time and a method for its approximate evaluation is proposed and justified. Section IV discusses the obtained results and their comparison to the experimental data available. The paper ends by overall con-

*Corresponding author. Email address: raikher@icmm.ru
†Also at Université Denis Diderot (Paris 7), UFR de Physique, 2 place Jussieu, 75251 Paris Cedex 05, France.

clusions and contains an appendix, where the main matrix equation, too long to be included in the text, is given.

II. GENERAL CONSIDERATIONS

In MFs the phenomenon of dynamic birefringence, as compared to conventional molecular optics, is somewhat unique. Indeed, a single-domain particle of nanoscopic size is superparamagnetic. That means that its magnetic moment is not rigidly bonded to the anisotropy (and thus, geometric) axis but is subjected to internal rotary diffusion. Hence, the response of a MF (as an assembly of such particles) to an external field is a combination of two relaxational processes. One is the orientation of the assembly of magnetic moments $\boldsymbol{\mu}$, i.e., the magnetization of the suspension. The other is the orientation of the particle axes $\boldsymbol{n}$, which strive to minimize the magnetic anisotropy energy by their mechanical rotation towards the new position of $\boldsymbol{\mu}$. This latter motion is in fact the direct cause of birefringence.

Being of different origins, those relaxational processes have different time scales. For the magnetic degrees of freedom in the absence of an external field, it is the time of internal superparamagnetic diffusion τ_D. For the mechanical ones it is the time of mechanical rotary diffusion τ_B of a particle in a carrier liquid. Remarkably, both parameters can be presented in a similar form [7],

$$\tau_B = 3\eta V/kT, \quad \tau_D = 3\eta_m V_m/kT, \tag{2}$$

where η is the viscosity of the carrier liquid, and kT is the temperature in energy units. If one conventionally describes the motion of the particle magnetic moment by the Landau-Lifshitz equation, the ''magnetic viscosity'' in Eq. (2) writes $\eta_m = I/6\alpha\gamma$, where γ is the gyromagnetic ratio for electrons and α the dimensionless rate of spin-lattice relaxation.

Let us define the orientation order parameter of a suspension in a tensor form as

$$S_{ik} = \frac{3}{2}\left[\langle n_i n_k\rangle - \frac{1}{3}\delta_{ik}\right], \tag{3}$$

assuming that the easy axis of the particle coincides with its optical axis. In a dilute suspension, the tensor S_{ik} is proportional to the refraction index tensor and, thus, determines the optical anisotropy of the particle assembly. Accordingly, the angular brackets in Eq. (3) denote statistical averaging with the orientational distribution function $W(\boldsymbol{e},\boldsymbol{n},t)$ of the particle. The evolution of this function is given by the extended Fokker-Planck equation, whose configurational space $\boldsymbol{e}\otimes\boldsymbol{n}$ is a direct product of two two-dimensional vector spaces. This equation was derived in Refs. [8–10] for arbitrary τ_B and τ_D. In the absence of a bulk flow of a MF it reads

$$\frac{\partial}{\partial t}W + \hat{\boldsymbol{J}}_{\boldsymbol{e}}\cdot\boldsymbol{\Omega}_L W = \left\{\frac{1}{2\tau_B}(\hat{\boldsymbol{J}}_{\boldsymbol{e}}+\hat{\boldsymbol{J}}_{\boldsymbol{n}})W(\hat{\boldsymbol{J}}_{\boldsymbol{e}}+\hat{\boldsymbol{J}}_{\boldsymbol{n}}) + \frac{1}{2\tau_D}\hat{\boldsymbol{J}}_{\boldsymbol{e}}W\hat{\boldsymbol{J}}_{\boldsymbol{e}}\right\}(U/kT + \ln W). \tag{4}$$

Here $\hat{\boldsymbol{J}}_{\boldsymbol{e}} = (\boldsymbol{e}\times\partial/\partial\boldsymbol{e})$ and $\hat{\boldsymbol{J}}_{\boldsymbol{n}} = (\boldsymbol{n}\times\partial/\partial\boldsymbol{n})$ are the operators of infinitesimal rotations in the corresponding vector spaces, and the precession (Larmor) frequency of the magnetic moment is defined in a vector form as

$$\boldsymbol{\Omega}_L = -(\gamma/IV_m)(\partial U/\partial\boldsymbol{e}).$$

In the absence of an external magnetic field, the solution of Eq. (4) factorizes as

$$W(\boldsymbol{e},\boldsymbol{n},t) = W_{\boldsymbol{e}}(\boldsymbol{e}\cdot\boldsymbol{n},t)W_{\boldsymbol{n}}(\boldsymbol{n},t), \tag{5}$$

where $W_{\boldsymbol{e}}$ is the orientational distribution of vector $\boldsymbol{e}$ with respect to the anisotropy axis $\boldsymbol{n}$ and $W_{\boldsymbol{n}}$ is the orientational distribution of vector $\boldsymbol{n}$ with respect to the laboratory coordinate framework. For representation (5) the equations that govern the distribution functions separate and become self-contained. The equation for the internal degrees of freedom is

$$2\tau_D \frac{\partial W_{\boldsymbol{e}}}{\partial t} = \hat{\boldsymbol{J}}_{\boldsymbol{e}}W_{\boldsymbol{e}}\hat{\boldsymbol{J}}_{\boldsymbol{e}}[-\sigma(\boldsymbol{e}\cdot\boldsymbol{n})^2 + \ln W_{\boldsymbol{e}}], \tag{6}$$

where $\sigma = E_a/kT$ is the height of the potential barrier of magnetic anisotropy scaled with temperature. For the distribution function of the external rotations one gets

$$2\tau_B \frac{\partial W_{\boldsymbol{n}}}{\partial t} = \hat{\boldsymbol{J}}_{\boldsymbol{n}}^2 W_{\boldsymbol{n}}, \tag{7}$$

which is a standard rotary diffusion equation. Both Eqs. (6) and (7) are well known in the theory of the rotary Brownian motion. The eigenfunctions of Eq. (7) are the ''external'' spherical harmonics, i.e., the functions of the angles that vector $\boldsymbol{n}$ makes with some axis of the laboratory coordinate framework that is defined by a unit vector $\boldsymbol{z}$,

$$W_{\boldsymbol{n}}(\vartheta,\phi,t) = \sum X_l^m(\boldsymbol{n},\boldsymbol{z})\exp[-l(l+1)t/\tau_B]. \tag{8}$$

For the solution of Eq. (6) the basis of ''internal'' spherical harmonics

$$W_{\boldsymbol{e}}(\theta,\varphi,t) = \sum_{l=0}^{\infty}\sum_{m=-l}^{l} b_{l,m}(t)\,\frac{2l+1}{4\pi} \times \frac{(l-|m|)!}{(l+|m|)!}\,X_l^{m*}(\boldsymbol{e},\boldsymbol{n}) \tag{9}$$

was proposed in Ref. [11]. In Eqs. (8) and (9) symbols $X_l^m(\boldsymbol{a},\boldsymbol{b})$ denote the so-called non-normalized spherical harmonics defined as

$$X_l^m(\boldsymbol{a},\boldsymbol{b}) = P_l^m(\cos\alpha)e^{im\beta}, \tag{10}$$

where P_l^m are the associated Legendre polynomials. The angles α and β are the coordinates of the unit vector $\boldsymbol{a}$ in the spherical framework with the polar axis set along the unit vector $\boldsymbol{b}$. Functions (10) are connected to the conventional, normalized, spherical harmonics by the relationship

$$Y_l^m = \sqrt{\frac{2l+1}{4\pi}\frac{(l-|m|)!}{(l+|m|)!}}\; X_l^m. \tag{11}$$

As soon as a magnetic field is applied, it couples the internal and external degrees of freedom of the particle, and the variables in the kinetic equation (4) become inseparable. Due to that, the solution should be constructed in the functional space formed by direct products of the ''internal'' and ''external'' harmonics. A suitable representation for this case is

$$W(\boldsymbol{e},\boldsymbol{n},t) = \sum_{l=1}^{\infty}\sum_{l'=1}^{\infty}\sum_{m=-l'}^{l'} Q_{l,l'}^{m,m'}(t)\frac{(2l+1)(l-|m|)!}{4\pi(l+|m|)!} \times X_l^{m*}(\boldsymbol{e},\boldsymbol{n})\;\frac{(2l'+1)(l'-|m'|)!}{4\pi(l'+|m'|)!}\;X_{l'}^{m'*}(\boldsymbol{n},\boldsymbol{h}), \tag{12}$$

where the time dependence is now determined by the four-index coefficients

$$Q_{l,l'}^{m,m'}(t) = \langle X_l^m(\boldsymbol{e},\boldsymbol{n})X_{l'}^{m'}(\boldsymbol{n},\boldsymbol{h})\rangle. \tag{13}$$

Note that vector $\boldsymbol{h}$, being imposed in the laboratory framework, in a natural way takes the place of the formerly arbitrary unit vector $\boldsymbol{z}$ in the subset of the ''external'' harmonics.

Substitution of expansion (12) in Eq. (4) and subsequent integration with respect to $\boldsymbol{e}$ and $\boldsymbol{n}$, results in an infinite set of differential recurrence relations from which the coefficients $Q_{l,l'}^{m,m'}$ may be found by a numerical procedure. The general form of the emerging set of equations is given in the Appendix. The quantity of our main interest there is the equation of motion for the element

$$Q_{0,2}^{0,1} = \langle 3\cos\vartheta\sin\vartheta\cos\phi\rangle, \tag{14}$$

which is the spherical representation of the only component of the orientation order parameter (3) excited by the probing field in the crossed-field configuration. As mentioned, it is proportional to the observed birefringence. Accordingly, its square is proportional to the registered intensity of the transmitted light.

III. HARD-DIPOLE PARTICLES

First, we consider a crossed-field birefringence in the framework of a simple model, where internal magnetic degrees of freedom are ''frozen,'' i.e., for the case of hard-dipole particles. This limit means that we set E_a in Eq. (1) to infinity, or, equivalently, set $\boldsymbol{e}=\boldsymbol{n}$ in the energy (1) reducing it to

$$U = -\mu H(\boldsymbol{e}\cdot\boldsymbol{h}), \tag{15}$$

where the value of the particle magnetic moment $\mu = IV_m$ is assumed to be constant. The stationary distribution function of an assembly of noninteracting magnetic moments in a constant field $\boldsymbol{H}_0 = H_0\boldsymbol{h}$ is determined by the Gibbs expression

$$W_0(\boldsymbol{e}) = \frac{\xi_0}{4\pi\sinh\xi_0}\exp[\xi_0(\boldsymbol{e}\cdot\boldsymbol{h})], \tag{16}$$

where the Langevin argument associated with the bias field H_0 is

$$\xi_0 = \mu H_0/kT. \tag{17}$$

For the hard-dipole case the Fokker-Planck equation (4) reduces to

$$2\tau_B\;\frac{\partial}{\partial t}\;W = \hat{\boldsymbol{J}}W\hat{\boldsymbol{J}}\left(\frac{U}{kT}+\ln W\right), \tag{18}$$

where the distribution function $W(\boldsymbol{e},t)$ does not depend on the anisotropy parameters and the rotation operator is $\hat{\boldsymbol{J}} \equiv \hat{\boldsymbol{J}}_{\boldsymbol{e}}$. Denoting the spherical coordinates of the unit vectors $\boldsymbol{e}$ and $\boldsymbol{h}$ as $(\theta,\ \varphi)$ and (0,0), respectively, one expands the solution of the kinetic equation (18) in spherical harmonics as

$$W(\theta,\varphi,t) = \sum_{l=0}^{\infty}\sum_{m=-l}^{l} b_{l,m}(t)\frac{2l+1}{4\pi} \times\frac{(l-|m|)!}{(l+|m|)!}\;X_l^{m*}(\boldsymbol{e},\boldsymbol{h}), \tag{19}$$

where the variables are separated and the time dependence is determined by the functions

$$b_{l,m}(t) = \langle P_l^m(\cos\theta)e^{im\varphi}\rangle, \tag{20}$$

with the angular brackets denoting statistical averaging with the distribution function W found from Eq. (18). Note that for hard dipoles, due to the reduction of the configurational space, we use a two-index notation $b_{l,m}$ instead of the general four-index one defined by Eq. (13).

As the probing field $\boldsymbol{H}$ is perpendicular to the bias field $\boldsymbol{H}_0$, the only nonzero perturbations are the functions $b_{l,1}$, which may be found from the chain-linked set

$$2\tau_B\frac{d}{dt}b_{l,1}+l(l+1)b_{l,1}-\frac{\xi_0}{(2l+1)}[(l+1)^2b_{l-1,1}-l^2b_{l+1,1}]$$

$$=\frac{l(l+1)}{2l+1}[(l+1)L_{l-1}(\xi_0)+lL_{l+1}(\xi_0)]\xi, \qquad (21)$$

obtained by substitution of expansion (19) into Eq. (18); here $\xi=\mu H/kT$ should be regarded as the dimensionless probing field. Of the whole set $\{b_{l,1}\}$ the issues of main interest are its first two components. Indeed, $b_{1,1}$ is the spherical representation of the normalized magnetization (perpendicular to $\boldsymbol{H}_0$) while $b_{2,1}$ is the spherical component of the orientation order parameter which is responsible for the optical birefringence excited by the probing field.

A. Weak bias field

Throughout this study we use the linear-response theory, assuming that the probing field is weak in the sense that the ratio $\xi=\mu H/kT$ is always much less than unity. As the starting point we set the bias to be weak as well, i.e., $\xi_0\sim\xi\ll 1$. Expanding the matrix set (21) to the next-to-the-lowest order in the field strengths (which means that we neglect $b_{3,1}$, $\xi b_{2,1}$, $\xi^2 b_{1,1}$, etc.) we arrive at a closed set of two equations,

$$\tau_B\frac{d}{dt}b_{1,1}+b_{1,1}=0, \quad \tau_B\frac{d}{dt}b_{2,1}+3b_{2,1}-\frac{9\xi_0}{10}b_{1,1}=0, \qquad (22)$$

which ties up the increments of magnetization and orientation. The initial conditions for this set are taken in the form

$$b_{1,1}(0)=\frac{2}{3}\xi, \quad b_{2,1}(0)=\frac{2}{5}\xi\xi_0, \qquad (23)$$

which means that the system dwells in equilibrium in the presence of the crossed fields $\boldsymbol{H}$ and $\boldsymbol{H}_0$ until the moment $t=0$ when $\boldsymbol{H}$ is turned off. For the corresponding transient process the solution of Eqs. (22) is

$$b_{1,1}(t)=\frac{2}{3}\xi e^{-t/\tau_B},$$

$$b_{2,1}(t)=\frac{1}{10}\xi\xi_0(3e^{-t/\tau_B}+e^{-3t/\tau_B}). \qquad (24)$$

Thus, one sees that the vector mode $b_{1,1}$ coincides with the eigenmode of the set (22), while the tensor mode $b_{2,1}$ turns out to be a superposition of two eigenmodes. Moreover, it turns up that $b_{2,1}(t)$, i.e., the field-induced birefringence in a suspension of hard dipoles, contains a considerable contribution that decays with the rate of the vector mode $b_{1,1}$, i.e., magnetization. This significant fact had been discovered quite a time ago in the molecular electro-optics, see the results of Ref. [12], where an obvious substitution of magnetization instead of electric polarization should be done.

As follows from Eqs. (24), even in a weak bias field, relaxation of birefringence is a multimode process. The more so this applies to the cases where the bias field is finite. A simple and convenient way to characterize and compare multimode processes is to use the so-called *integral relaxation time* (IRT). For a decay process it is defined as the time integral of the response function under study taken from the moment $t=0$ to infinity and divided by the value of the relaxing quantity at $t=0$,

$$\tau_{\rm int}^{(l)}=[b_{l,1}(0)]^{-1}\int_0^\infty b_{l,1}\ dt. \qquad (25)$$

A significant merit of IRT is that it incorporates contributions of all the modes of the system spectrum. As mentioned, the subjects of our interest are the modes with $l=1$ (vector) and $l=2$ (second-rank tensor). Applying definition (25) to the transient processes described by Eqs. (24), we find

$$\tau_{\rm int}^{(1)}=\tau_B, \quad \tau_{\rm int}^{(2)}=\frac{5}{6}\tau_B. \qquad (26)$$

It is worthwhile to remark once again the difference with the case of a field-free ($\xi_0=0$) system, where all the relaxation eigenmodes decouple. There the integral times coincide with the inverses of the respective eigenvalues and instead of Eqs. (26) one has $\tau_{\rm int}^{(1)}=\tau_B$ and $\tau_{\rm int}^{(2)}=\tau_B/3$. Formally this means that in a field-free system birefringence decays 2.5 times faster than in a system with an applied bias field, however weak the latter is. This is a well-known paradox in orientational optics of dipolar systems found and elucidated by Ullman, see Ref. [12]. Not repeating the exhaustive explanation given in the original paper, we just remind its key point: with $\xi_0\to 0$ the initial condition (23) for the orientation order parameter $b_{2,1}$ also tends to zero. In other words, at $\xi_0=0$ there is no linear contribution in birefringence, this rapidly decaying mode does not exist without ξ_0. In the zero bias (field-free) case the birefringence expansion begins with the term quadratic in the probing field ξ, and this perturbation indeed decays with the time $\tau_B/3$.

B. Arbitrary bias field

If the bias field is not weak, the evolution of any $b_{l,1}$ becomes a multimode process. However, for the vector (magnetization) mode a good single-time approximation is provided by the expression

$$\tau_{\rm eff}^{(1)}=\frac{2L_1(\xi_0)}{\xi_0-L_1(\xi_0)}\ \tau_B, \qquad (27)$$

derived in Ref. [13]; here L_1 is the Langevin function.

Let us obtain a similar characteristic for the tensor (orientation order parameter) mode using the concept of the integral relaxation time introduced by Eq. (25). To do that, it is convenient to perform time integration of Eq. (21). Setting there $\xi=0$ (the probing field switched off), one gets

$$2\tau_B b_{l,1}(0)=l(l+1)F_l-\frac{\xi_0}{(2l+1)}[(l+1)^2F_{l-1}-l^2F_{l+1}], \qquad (28)$$

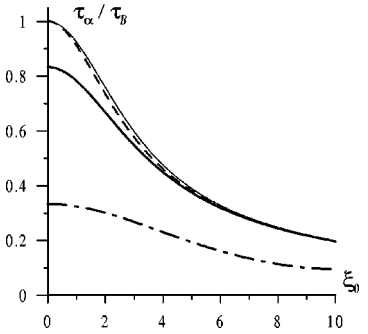

FIG. 1. Comparison of the characteristic relaxation times. Dashed curve, the effective relaxation time $\tau_{\rm eff}^{(1)}$ of magnetization according to Eq. (27); thin solid curve, integral relaxation time $\tau_{\rm int}^{(1)}=F_1/b_{1,1}(0)$ of magnetization (mode $b_{1,1}$); thick solid curve, integral relaxation time $\tau_{\rm int}^{(2)}$ of the orientation order parameter (mode $b_{2,1}$); dashed-dotted curve, relaxation time of the second eigenmode of Eq. (21).

where we denote

$$F_l \equiv \int_0^\infty b_{l,1}\ dt. \tag{29}$$

The left-hand side of Eq. (28) is built of the initial condition, i.e., is determined by an equilibrium average over the initial state of the system, where both $\boldsymbol{H}_0$ and $\boldsymbol{H}$ exist. For small probing fields, expansion with respect to ξ yields

$$b_{l,1}(0)=l(l+1)L_l(\xi_0)(\xi/\xi_0), \tag{30}$$

where L_l is the Langevin function of l order defined as

$$L_l=Z_L^{-1}\int_{-1}^{1}P_l(x)\exp(\xi_0 x)dx, \quad Z_L=\sinh\xi_0/\xi_0.$$

With the same accuracy in ξ, the coefficients F_l defined by Eq. (29) may be presented in the form $F_l=\xi f_l$, where now functions $f(\xi_0)$ do not depend on ξ. Then the set (28) rewrites as

$$2\tau_B l(l+1)\frac{L_l(\xi_0)}{\xi_0}=l(l+1)f_l-\frac{\xi_0}{(2l+1)}[(l+1)^2 f_{l-1} - l^2 f_{l+1}], \tag{31}$$

and is solved numerically by the continuous fraction method, as described in Ref. [14]. For $l=2$, the integral relaxation time (25) in view of Eq. (30) takes the form

$$\tau_{\rm int}^{(2)}=\frac{\xi_0 f_2}{6L_2(\xi_0)}\ \tau_B. \tag{32}$$

Since the orientation relaxation time $\tau^{(2)}$ was derived in the linear-response approximation, Eq. (32) is equally appropriate for the situations where the probing field is turned on.

The numerical results for the integral relaxation times as the functions of the bias-field strength are presented in Fig. 1, together with the effective dipole (vector) relaxation time (27). One sees that at small ξ_0 (weak fields and/or high temperatures) the limit of the integral relaxation time of birefringence is $\tau_{\rm int}^{(2)}=5\tau_B/6$, as given by Eq. (26). This results from transforming via Eq. (25) the superposition (24) of the two eigenmodes of the set (22). At $\xi_0\to 0$ the decay times (inverse eigenvalues) of these modes are, respectively, τ_B and $\tau_B/3$; their relative weights (components in the eigenvector space) in the tensor mode $b_{2,1}$ are 3/4 and 1/4. (As mentioned, in this approximation the first eigenmode coincides with the vector mode $b_{1,1}$.) Under the bias field, both the eigenvalues and eigenvectors change, causing the changes of the integral times. In Fig. 1 the curve rendering the ξ_0 dependence of the integral relaxation time for the first eigenmode and the line $\tau_{\rm eff}^{(1)}$ practically overlap. The relaxation time of the second eigenmode is shown in Fig. 1 by a dashed-dotted line. Monotonically with ξ_0, the contribution of the first eigenmode to the tensor mode $b_{2,1}$ grows so that at high ξ_0 (high magnetic fields and/or low temperatures) the integral time of orientation approaches $\tau_{\rm int}^{(1)}$ and $\tau_{\rm eff}^{(1)}$ so that all three curves unite at the same asymptote $\propto\tau_B/\xi_0$. Therefore, one concludes that in a suspension of hard dipoles under the crossed-field configuration with the decrease of fluctuations the relaxation rate of the orientation (birefringence) coincides with that of the magnetization.

IV. DIPOLAR PARTICLES WITH FINITE MAGNETIC ANISOTROPY

Now we proceed to the principal issue of the study: the dynamic birefringence in an assembly of nanoparticles with finite magnetic anisotropy that is subjected to a combination of a constant (bias) and a pulse or ac (probing) magnetic fields. This case is described by the general Fokker-Planck equation (4) whose solution is presented by expansion (12). As mentioned at the end of Sec. II, we focus on the equation for the orientation order parameter $Q_{0,2}^{0,1}$. Extracting the pertinent line from the complete set of matrix equations, see Eq. (A1) of the Appendix, we get

$$2\tau_B\frac{d}{dt}Q_{0,2}^{0,1}+6Q_{0,2}^{0,1}-\frac{\xi_0}{5}(9Q_{1,1}^{0,1}+9Q_{1,1}^{1,0}-4Q_{1,3}^{0,1}+6Q_{1,3}^{1,0})=0. \tag{33}$$

As in the above, we assume that the actual relaxation process is a switch off of the probing field so that the system evolves from the equilibrium state, where both $\boldsymbol{H}_0$ and $\boldsymbol{H}$ existed, to another equilibrium, where only $\boldsymbol{H}_0$ remains. The corresponding initial condition in a suspension of particles with a finite magnetic anisotropy is

$$Q_{0,2}^{0,1}(0)=6S_2(\sigma)L_2(\xi_0)(\xi/\xi_0), \tag{34}$$

cf. Eq. (30). Here S_2 is the ''intraparticle'' order parameter that describes the orientation of the axis $\boldsymbol{n}$ with respect to the magnetic moment $\boldsymbol{e}$. One may also say that S_2 is the order parameter in a suspension where the particle magnetic moments are perfectly aligned by an infinitely strong magnetic field. A simple representation for S_2 is

$$S_2=\frac{3}{2}\left(\frac{d}{d\sigma}\ln R-\frac{1}{3}\right),\quad R(\sigma)=\int_0^1\exp(\sigma y^2)dy, \quad (35)$$

which follows from the general definition

$$S_{2l}=R^{-1}\int_0^1 P_{2l}(y)\exp(\sigma y^2)dy. \quad (36)$$

A. Weak bias field

Let us start with the case of a weak bias field. Estimations by the order of magnitude show that in this limit in Eq. (33) the terms $Q_{1,3}$ should be omitted, so that the mode $Q_{0,2}^{0,1}$ remains coupled to $Q_{1,1}^{0,1}$ and $Q_{1,1}^{1,0}$. The equations for the latter follow from the general matrix equation (A1) and were derived in Refs. [9,10]. Uniting all the equations, we get a closed set that describes dynamic birefringence in the crossed-field configuration,

$$\tau_\parallel\ \frac{d}{dt}Q_{1,1}^{0,1}+Q_{1,1}^{0,1}=0,\quad \tau_\perp\frac{d}{dt}Q_{1,1}^{1,0}+Q_{1,1}^{1,0}=0,$$

$$2\tau_B\frac{d}{dt}Q_{0,2}^{0,1}+6Q_{0,2}^{0,1}=\frac{9\xi_0}{5}(Q_{1,1}^{0,1}+Q_{1,1}^{1,0}). \quad (37)$$

Here the relaxation times are the effective parameters incorporating contributions from the diffusion with respect to both external (mechanical) and internal (magnetic) rotary degrees of freedom of the particles. They are defined as

$$\tau_\parallel^{-1}=\tau_B^{-1}+\tau_{10}^{-1},\quad \tau_\perp^{-1}=\tau_B^{-1}+\tau_{11}^{-1}. \quad (38)$$

For them simple but fairly good approximations have been developed. In particular, we take

$$\tau_{10}=\tau_D\ \frac{e^\sigma-1}{2\sigma}\left(\frac{\sqrt{\pi\sigma}}{1+\sigma}+2^{-\sigma-1}\right)^{-1}, \quad (39)$$

$$\tau_{11}=2\tau_D\ \frac{1-S_2}{2+S_2},$$

as proposed in Refs. [15] and [8], respectively.

The initial conditions for the set (37) determined with the appropriate accuracy write

$$Q_{1,1}^{0,1}(0)=\frac{2}{3}\chi_\parallel\xi,\quad Q_{1,1}^{1,0}(0)=\frac{4}{3}\chi_\perp\xi,\quad Q_{0,2}^{0,1}(0)=\frac{2}{5}S_2\xi\xi_0, \quad (40)$$

where the components of the particle magnetization are presented with the aid of the corresponding static magnetic susceptibilities:

$$\chi_\parallel=\frac{1}{3}(1+2S_2),\quad \chi_\perp=\frac{1}{3}(1-S_2). \quad (41)$$

The indices here refer to the direction of the probing field $\boldsymbol{H}$ with respect to the anisotropy axis of the particle. Note also that thus defined χ do not depend on the bias field.

From Eqs. (37) and (40) one sees that with respect to the fields the orientational order parameter $Q_{0,2}^{0,1}$ scales as $\xi\xi_0$. The sum $(Q_{1,1}^{0,1}+Q_{1,1}^{1,0})$, which scales as ξ, enters the equation for $Q_{0,2}^{0,1}$ multiplied by ξ_0 and plays there the role of a driving force. Therefore, both magnetization components, longitudinal and transverse with respect to the anisotropy axis, affect $Q_{0,2}^{0,1}$. This fact is easy to understand if one recalls that in our study the laboratory framework is built on the directions of the bias and probing fields and not on the internal axes of the particles. Entering the equation in a symmetrical way, the magnetization modes have different relaxation properties as follows from expressions (38) and (39).

Let us first consider the motion of $Q_{1,1}^{1,0}$. From Eqs. (35) and (39) it follows that τ_{11} never exceeds τ_D. In turn, the latter is rather short in comparison with τ_B. Thence, according to the second of Eqs. (38), the relaxation time $\tau_\perp$ is always of the order of τ_D or less (for $\sigma\gg1$).

The effect of motion of the component $Q_{1,1}^{0,1}$ is quite different due to the time τ_{10} that enters the expression for $\tau_\parallel$. Recalling that $Q_{1,1}^{0,1}$ characterizes the perturbation of the particle magnetization that is parallel to the anisotropy axis, one recognizes in τ_{10} at $\sigma>1$ the activation-type time of the Néel superparamagnetism. Due to the exponential dependence, τ_{10} changes dramatically with temperature and, as the latter goes down, passes from a fast isotropic diffusion of the vector $\boldsymbol{e}$, where $\tau_{10}\sim\tau_D$, to the regime of completely frozen-in magnetic moment ($\tau_{10}\to\infty$). In the intermediate temperature range τ_{10} may become comparable with τ_B, thus changing considerably the effective time $\tau_\parallel$. However, due to the exponential factor in the function τ_{10} the range of comparability is very narrow. In other words, almost always only one of the two regimes is possible: either σ is small yielding $\tau_{10}\sim\tau_D$ that leads to $\tau_\parallel\sim\tau_D\ll\tau_B$ or σ is large, and one has $\tau_\parallel\sim\tau_B$.

Solving Eqs. (37) with initial conditions (40) for a switch-off process, one finds

$$Q_{0,2}^{0,1}(t)=\frac{1}{5}\ \xi\xi_0\left\{\frac{3\chi_\parallel\tau_\parallel}{3\tau_\parallel-\tau_B}e^{-t/\tau_\parallel}+\frac{6\chi_\perp\tau_\perp}{3\tau_\perp-\tau_B}e^{-t/\tau_\perp}\right.$$
$$\left.+\left[2S_2-\frac{3\chi_\parallel\tau_\parallel}{3\tau_\parallel-\tau_B}-\frac{6\chi_\perp\tau_\perp}{3\tau_\perp-\tau_B}\right]e^{-3t/\tau_B}\right\}. \quad (42)$$

The limiting cases of Eq. (42) can be considered using the relations

$$\tau_\parallel=\tau_\perp=\tau_D\quad \text{for}\ \ \sigma\ll1,$$

$$\tau_\parallel=\tau_B,\quad \tau_\perp=\tau_D\quad \text{for}\ \ \sigma\gg1. \quad (43)$$

In particular, one finds that at $\sigma\to\infty$ formula (42) transforms into expression (24) obtained for a MF of magnetically hard particles if one sets $b_{2,1}=Q_{0,2}^{0,1}$.

The integral relaxation time for the process described by Eq. (42) is found via definition (25) and writes

$$\tau_{\rm int}^{(2)}=\frac{\tau_B}{3}+\frac{\chi_\parallel\tau_\parallel+2\chi_\perp\tau_\perp}{2S_2}\simeq\frac{\tau_B}{3}+\frac{\chi_\parallel\tau_\parallel}{2S_2}, \quad (44)$$

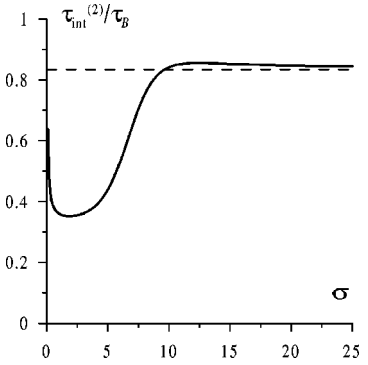

FIG. 2. Integral relaxation time under weak bias field as a function of σ by Eq. (44), horizontal asymptote is $\tau_{\rm int}^{(2)}/\tau_B = 5/6$; for an explanation of the behavior in the small σ range see the text.

where the last simplification is justified due to the smallness of $\chi_\perp \tau_\perp$ in comparison to the respective longitudinal combination. In Fig. 2 we plot $\tau_{\rm int}^{(2)}$ calculated numerically. To compare the exact curve with the asymptotic estimations, let us apply to Eq. (44) relations (43) and then tend to the low frequency or ''kinetic cutoff'' limit, i.e., set $\tau_D = 0$. This gives

$$\tau_{\rm int}^{(2)} = \tau_B \begin{cases} 1/3 & \text{for } \sigma \ll 1, \\ 5/6 & \text{for } \sigma \gg 1. \end{cases} \tag{45}$$

From Fig. 2 one sees that at the high anisotropy end ($\sigma \gg 1$) the curve behaves as expected: it tends to the hard-dipole regime with $\tau_{\rm int}^{(2)} = 5\tau_B/6$, see Eq. (26). From closer inspection it follows that at certain σ the relaxation time $\tau_{\rm int}^{(2)}$ passes through a weak maximum and then approaches the limiting value from above. At σ tending to zero the numerically evaluated curve first tends to 1/3, as predicted by Eq. (45), but then inflects and begins to ascend. The occurring minimum does not have any physical meaning though. It is just an indication that our definition of IRT does not apply to the case because when exciting an assembly of perfectly magnetically isotropic particles by a pulse field, both initial and final orientational order parameters are zeros. However, the estimations done at $\sigma \ll 1$ prove that as long as the particle magnetic anisotropy satisfies the condition $\sigma \gtrsim \tau_D/\tau_B \ll 1$, the limit given by the first line of Eq. (45) remains valid.

We remark that the approximation we deal in allows in full for the fact that the profile of the magnetic potential energy of the particle consists of two wells of equal depth, and the magnetic moment may occupy either of them. In other words, both the interwell and intrawell transitions of the magnetic moment are accounted for. On the other hand, the effect of the external field on the particle potential energy is neglected here.

B. Strong bias field

Another limiting case is the one where the bias field H_0 is strong and, in particular, stronger than the anisotropy field $H_a = 2E_a/IV_m$. Under this condition, the profile of the magnetic potential energy of the particle has only one minimum. This justifies the possibility to take the solution of Eq. (4) in the form of a trial function

$$W(\boldsymbol{e},\boldsymbol{n},t) = W_0[1 + a_1(t)X_1^1(\boldsymbol{e},\boldsymbol{h}) + a_2(t)X_2^1(\boldsymbol{n},\boldsymbol{h})], \tag{46}$$

as is done in the effective-field method [7]; here a_i are the adjustable parameters. In Eq. (46) the equilibrium distribution function W_0 is defined with the energy (1) in the full configurational space of the system,

$$W_0 = Z^{-1}\exp[\xi_0(\boldsymbol{e}\cdot\boldsymbol{h}) + \sigma(\boldsymbol{e}\cdot\boldsymbol{n})^2], \tag{47}$$

$$Z = 16\pi^2 R(\sigma)\frac{\sinh\xi_0}{\xi_0}.$$

In view of Eq. (46), the first two moments of the nonequilibrium distribution function, which are the principal items of the study, write

$$Q_1 \equiv \langle X_1^1(\boldsymbol{e},\boldsymbol{h})\rangle, \quad Q_2 \equiv \langle X_2^1(\boldsymbol{n},\boldsymbol{h})\rangle. \tag{48}$$

Here in the notations for Q we have reduced the number of indices to the necessary minimum and will use this convention from now on.

Substituting expansion (46) in Eqs. (48), one gets a 2×2 matrix relationship,

$$Q_i = N_{ik}a_k, \tag{49}$$

which expresses the observable statistical moments via the effective fields. The coefficients in Eq. (49) are

$$N_{11} = \langle X_1^1(\boldsymbol{e},\boldsymbol{h})X_1^{-1}(\boldsymbol{e},\boldsymbol{h})\rangle_0 = (2/\xi_0)L_1(\xi_0),$$

$$N_{12} = N_{21} = \langle X_1^1(\boldsymbol{e},\boldsymbol{h})X_2^{-1}(\boldsymbol{n},\boldsymbol{h})\rangle_0 = (6/\xi_0)L_2(\xi_0)S_2(\sigma), \tag{50}$$

$$N_{22} = \langle X_2^1(\boldsymbol{n},\boldsymbol{h})X_2^{-1}(\boldsymbol{n},\boldsymbol{h})\rangle_0 = (6/35)[7 + 5L_2(\xi_0)S_2(\sigma) - 12L_4(\xi_0)S_4(\sigma)],$$

where the angular brackets denote averaging over the equilibrium distribution (47).

The equations for the longitudinal (with respect to the bias field) component of the magnetic moment (Q_1) and for the component of the orientational order parameter in the same direction (Q_2) follow from Eq. (4) on substituting there the effective-field expansion (46), multiplying it from the left by first X_1^1 and then X_2^1 and performing integrations. By that, one arrives at the relationship

$$\frac{d}{dt}Q_i = -\Gamma_{ik}a_k, \tag{51}$$

with the following matrix of the kinetic coefficients:

$$\Gamma_{11} = \left(\frac{1}{2\tau_B} + \frac{1}{2\tau_D}\right)\langle[\hat{\boldsymbol{J}}_{\boldsymbol{e}}X_1^1(\boldsymbol{e},\boldsymbol{h})][\hat{\boldsymbol{J}}_{\boldsymbol{e}}X_1^{-1}(\boldsymbol{e},\boldsymbol{h})]\rangle_0 = \left(\frac{1}{\tau_B} + \frac{1}{\tau_D}\right)\frac{2+L_2(\xi_0)}{3},$$

$$\Gamma_{12} = \Gamma_{21} = \frac{1}{\tau_B}\langle[\hat{\boldsymbol{J}}_{\boldsymbol{e}}X_1^1(\boldsymbol{e},\boldsymbol{h})][\hat{\boldsymbol{J}}_{\boldsymbol{n}}X_2^{-1}(\boldsymbol{n},\boldsymbol{h})]\rangle_0 = \frac{3}{\tau_B}\ S_2(\sigma)\frac{3L_1(\xi_0)+2L_3(\xi_0)}{5}, \tag{52}$$

$$\Gamma_{22} = \langle[\hat{\boldsymbol{J}}_{\boldsymbol{n}}X_2^1(\boldsymbol{n},\boldsymbol{h})][\hat{\boldsymbol{J}}_{\boldsymbol{n}}X_2^{-1}(\boldsymbol{n},\boldsymbol{h})]\rangle_0 = \frac{9}{\tau_B}\ \frac{14+5L_2(\xi_0)S_2(\sigma)+16L_4(\xi_0)S_4(\sigma)}{35}.$$

Eliminating the effective fields a_i from Eq. (51) with the aid of Eq. (49), one arrives at the closed matrix relaxation equation

$$\frac{d}{dt}\ Q_i = -\Gamma_{il}N_{lk}^{-1}Q_k, \tag{53}$$

for which the initial conditions describing a switch off of the probing field are

$$Q_1(0) = N_{11}\xi, \quad Q_2(0) = N_{12}\xi. \tag{54}$$

Solution of Eq. (53) yields two eigenmodes, whose relaxation times are ''mixtures'' of τ_B and τ_D. Using once again the definition of IRT, we derive the expression for the integral relaxation time of the orientation order parameter in the form

$$\tau_{\rm int}^{(2)}(\xi_0,\sigma) = \frac{\Gamma_{11}N_{22}N_{12}+\Gamma_{22}N_{11}N_{12}-\Gamma_{12}(N_{11}N_{22}+N_{12}^2)}{(\Gamma_{11}\Gamma_{22}-\Gamma_{12}^2)N_{12}}, \tag{55}$$

where the coefficients N_{ik} and Γ_{ik} are determined by formulas (50) and (52), respectively.

A useful simplification of the obtained formula is to tend to zero the ratio

$$\varepsilon = \tau_D/\tau_B = \eta_m/\eta = I/6\alpha\gamma\eta \tag{56}$$

of the magnetic to usual viscosities, see Eqs. (2). Actually, in experiments with magnetic suspensions one is close enough to this situation. Indeed, substituting in Eq. (56) the typical values $I = 500$ G and $\gamma = 1.7\times10^7$ $\mathrm{Oe}^{-1}\,\mathrm{s}^{-1}$, we arrive at the estimate

$$\varepsilon = 5\times10^{-6}/\alpha\eta,$$

which depends on the material constants α and η of a particular sample. The values of α in dispersed particles are usually about 0.01–0.1, sometimes rising to several tens of percent. The fluid viscosity η ranges from 10^{-2} to 10 Ps, thus covering a variety of fluids from water to glycerine. Combining these numbers, we see that the corresponding values of ε fall between 5×10^{-6} and 5×10^{-2}, always remaining far less than unity. Under this condition, Γ_{11} appears, see Eqs. (52), to be the sole leading term. Tending it to infinity reduces Eq. (55) to

$$\tau_{\rm int}^{(2)}(\xi_0,\sigma) = \frac{N_{22}}{\Gamma_{22}} = \frac{2}{3}\tau_B\frac{7+5L_2(\xi_0)S_2(\sigma)-12L_4(\xi_0)S_4(\sigma)}{14+5L_2(\xi_0)S_2(\sigma)+16L_4(\xi_0)S_4(\sigma)}. \tag{57}$$

This formula yields the relaxation time of the orientational order parameter in the case of a MF, in which particles have zero magnetic viscosity. The latter means that any transient rotation of the magnetic moment does not to a slightest extent entrain the body of the particle and vise versa. That is why we term this kinetic decoupling of the vectors $\boldsymbol{e}$ and $\boldsymbol{n}$ a ''cutoff.'' Actually, the ''kinetic cutoff'' limit is applicable to the processes whose reference times are much longer than τ_D. Then one may consider that with respect to the internal degrees of freedom the equilibrium is attained in zero time. Note that Eq. (57) can be obtained straightforwardly if one takes the trial function in a simplified form: setting $a_1 = 0$ in Eq. (47), thus assuming instantaneous magnetic relaxation. This approximation was used by Cebers in Ref. [18]. One has to understand clearly, however, that the kinetic freedom of a magnetic moment does not at all mean a complete breakdown of its orientational interaction with the anisotropy (geometry) axis. The equilibrium part of this interaction that is described by the cross term $\propto(\boldsymbol{e}\cdot\boldsymbol{n})^2$ in the particle energy (1), can be arbitrarily strong even at $\varepsilon = 0$.

At the first sight, the relaxation time $\tau_{\rm int}^{(2)}$ given by formula (55) or (57) seems to depend on both the bias field ξ_0 and the anisotropy parameter σ as if on independent variables. However, it is not entirely so. Being derived in the framework of the effective-field method, these formulas remain correct only in the range $\xi_0 > 2\sigma$, i.e., when the absence of magnetic metastability in the particle is ensured. That is why, for example, by tending $\sigma\to\infty$ whilst keeping ξ_0 finite, one never gets the relaxation time for a hard-dipole particles given by Eq. (27). However, for magnetically soft particles the ''kinetic cutoff'' approximation (57) has all the grounds to be quite useful.

In this connection we remark that a model similar to Eq. (51) has been proposed in Ref. [19] and applied there to account for the bias-field dependencies of the orientational relaxation time. Being justified in the range $\xi_0 > 2\sigma$, when used unmodified beyond this limit it did not render reasonable results.

C. Arbitrary bias field: Heuristic model

To get a description for the birefringence of a MF with arbitrary relation between the material parameters, one has to be able to solve the full set of equations (A1) for whatever ξ_0 and σ. This work, although it does not seem fundamentally impossible, would require a really huge amount of time and computer resources. This compels us to try to simplify the task, making use of certain qualitative considerations.

We base the model on the following heuristic grounds. As already mentioned, of the magnetization modes affecting birefringence one is rather fast and due to that does not contribute to the relaxation of the orientation order parameter. With allowance for this fact, the set (53) was reduced to just two equations. In the latter all the contribution of the internal magnetic mode is ''embodied'' in the relaxation time τ_D that enters the element Γ_{11} of the relaxation matrix Γ_{ik}, see Eqs. (52). Leaving all the formal scheme of Eqs. (46)–(56) intact, we account for the consequences of the possible magnetic metastability making in Γ_{11} just one replacement. Namely,

$$\tau_D \;\Rightarrow\; \widetilde{\tau}_D(\xi_0,\sigma) \equiv \tau_{\rm int}^{(1)}, \tag{58}$$

where $\tau_{\rm int}^{(1)}$ is the integral relaxation time for the longitudinal magnetization of a uniaxial superparamagnetic particle in the case, where the direction of $\boldsymbol{H}_0$ coincides with that of $\boldsymbol{n}$. This quantity determined numerically in Ref. [16] is plotted in Fig. 3 as a function of the dimensionless parameter $1/\sigma \propto T$ and the temperature-independent argument $\xi_0/\sigma \propto H_0$. In weak external fields the dependence $\widetilde{\tau}_D(1/T)$ closely resembles the usual Néel exponential ascend. As the bias field ξ_0 grows, the steepness of the increase gradually goes down. We remark that one of the prototypes of the function $\tau_{\rm int}^{(1)}$ was proposed in Ref. [17].

Making replacement (58) in Eq. (56), one arrives at the effective parameter $\widetilde{\varepsilon}(\xi_0,\sigma) = \widetilde{\tau}_D/\tau_B$. Unlike the seeding value ε that, as mentioned, in all physically meaningful situations is small, the modified $\widetilde{\varepsilon}$ can be of arbitrary magnitude. Apparently, small $\widetilde{\varepsilon}$ mean magnetic softness of the particles while large $\widetilde{\varepsilon}$ correspond to hard magnetic dipoles. Introducing this effective parameter in the element Γ_{11} and, accordingly, by means of Eq. (55), in the integral relaxation time, one can present the latter in the form

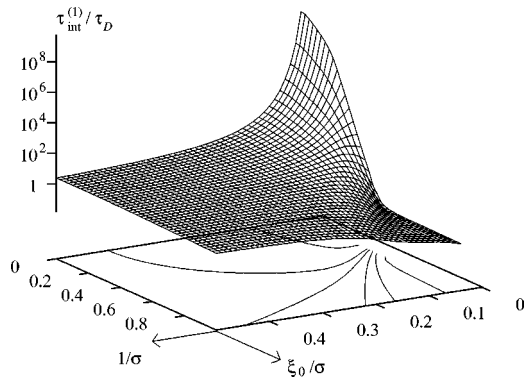

FIG. 3. Integral relaxation time of magnetization as a function of the dimensionless temperature $1/\sigma$ and bias-field strength ξ_0/σ, after Ref. [16].

$$\tau_{\rm int}^{(2)} = \frac{\psi_1 + \widetilde{\varepsilon}\,\psi_2}{\psi_3 + \widetilde{\varepsilon}\,\psi_4}\;\tau_B, \tag{59}$$

where expressions for the dimensionless functions $\psi_{1\text{–}4}(\xi_0,\sigma)$ follow from Eqs. (50) and (52). Since all ψ_i are constructed of nonsingular functions $L_k(\xi_0)$ and $S_k(\sigma)$, where $k = 2,4$, the relaxation time given by expression (59) is of the order of τ_B or, at strong bias fields, τ_B/ξ_0. The limiting forms follow from expanding Eq. (59) with respect to $\widetilde{\varepsilon}$,

$$\frac{\tau_{\rm int}^{(2)}}{\tau_B} = \begin{cases} \dfrac{\psi_1}{\psi_3}\left[1 + \widetilde{\varepsilon}\left(\dfrac{\psi_2}{\psi_1} - \dfrac{\psi_4}{\psi_3}\right)\right] \to \dfrac{\psi_1}{\psi_3} & \text{for } \widetilde{\varepsilon} \ll 1, \\ \dfrac{\psi_2}{\psi_4}\left[1 + \dfrac{1}{\widetilde{\varepsilon}}\left(\dfrac{\psi_1}{\psi_2} - \dfrac{\psi_3}{\psi_4}\right)\right] \to \dfrac{\psi_2}{\psi_4} & \text{for } \widetilde{\varepsilon} \gg 1. \end{cases} \tag{60}$$

The first line of this formula corresponds to the case of weak kinetic coupling, and, as it should be, its limit at $\widetilde{\varepsilon} = 0$ coincides with expression (57) obtained in a plain effective-field approximation. Note that at low σ the renormed $\widetilde{\varepsilon}$ does not differ much from real ε that is small. Besides, at low σ the condition $\xi_0 > 2\sigma$ is satisfied for low enough ξ_0. With regard to both those circumstances we conclude that the ''kinetic cutoff'' limit given by Eq. (57) works for practically any ξ_0. Changing it for the first line of Eq. (60) makes the expression just a bit more accurate.

The second line of Eq. (60), if to write it explicitly in terms of $L_k(\xi_0)$ and $S_k(\sigma)$ functions through Eqs. (50) and (52), is rather cumbersome. The limiting behavior at $\widetilde{\varepsilon} = \infty$ is rendered by the formulas

$$\left.\frac{\tau_{\rm int}^{(2)}}{\tau_B}\right|_{\widetilde{\varepsilon}=\infty} = \begin{cases} \dfrac{5}{6} - \left[\dfrac{31}{420} + \dfrac{S_2(\sigma)}{252} - \dfrac{S_2^2}{40}\right]\xi_0^2 + O(\xi_0^4) & \text{for } \xi_0 \ll 1, \\ \dfrac{2}{\xi_0} + \dfrac{6S_2}{6S_2 - \sigma(2 + S_2 - 3S_2^2)}\;\dfrac{1}{\xi_0^2} + O(1/\xi_0^3) & \text{for } \xi_0 \gg 1. \end{cases} \tag{61}$$

They prove that for both ξ_0 small and large the function (61) is very close to that describing the bias-field dependence of the birefringence relaxation time in a MF of hard dipoles. Moreover, the undertaken numeric calculations show that these functions stay close at any σ as well.

Since formula (59) proves to have a correct behavior in all the relevant limiting cases, we consider it to be a reasonable interpolation expression for arbitrary ξ_0 and σ including the range of magnetic metastability, where $\xi_0 < 2\sigma$. At $\tilde{\varepsilon} \sim 1$ a specific crossover in the dependence $\tau_{\rm int}^{(2)}(\xi_0)$ should occur: the hard-dipole behavior at $\tilde{\varepsilon} \gg 1$ changes for the "kinetic cutoff" one at $\tilde{\varepsilon} \ll 1$. Examples of the dependencies obtained with the aid of Eq. (59) are given in Fig. 4 as two families of curves differing by the value of the seeding kinetic coupling parameter ε. The graphs confirm the reliability of the constructed interpolation in more detail. At $\sigma \sim 1$ and lower (almost isotropic particles) the curves just slightly deviate from the asymptotic result $\tau_{\rm int}^{(2)}(\xi_0,0) = \tau_B/3$, that would have made a horizontal line in the plots. At high anisotropy ($\sigma \gg 1$), the curves closely approach the dotted contour that reflects the hard-dipole limit. Positioning of the starting (at $\xi_0 = 0$) points of all the curves inside the interval marked by the starting points of the limiting (marker) contours proves that however small τ_D (or corresponding ε) may be, its presence is crucial to obtain a correct relaxation time at large σ. Indeed, for a finite τ_D the time $\tilde{\tau}_D$ at low bias fields due to the exponential dependence incorporated in $\tau_{\rm int}^{(1)}$, see Fig. 3, at $\sigma \sim \ln(1/\varepsilon)$ by the order of magnitude reaches τ_B. Compare, for example, respective curves 2 in Figs. 4(a) and 4(b). For the particles with $\varepsilon = 10^{-3}$ the anisotropy parameter $\sigma = 5$ is yet too small, and the starting point of curve 2 in Fig. 4(a) virtually coincides with the value 1/3 yield by the "kinetic cutoff" limit. At the same value of σ, curve 2 in Fig. 4(b), i.e., for $\varepsilon = 10^{-2}$, branches off the vertical axis at a value that exceeds the asymptotic result by about 20%. For respective curves 3 corresponding to $\sigma = 10$ the effect is yet more pronounced. Here the curve for $\varepsilon = 10^{-3}$ starts already at the value that is considerably higher than 1/3, but on the other hand, it still remains well below the curve that describes the case $\varepsilon = 10^{-2}$. At yet higher σ, see the respective curves 4, the starting point of the function $\tau_{\rm int}^{(2)}(0,\sigma)/\tau_B$ approaches and then becomes indistinguishable from the hard-dipole result that equals 5/6, see Eq. (26). On the contrary, the starting point for the integral relaxation time in the "kinetic cutoff" limit (when one sets $\varepsilon \equiv 0$) never exceeds 1/3 however high σ may be, see diamond markers at $\xi_0 = 0$ in Figs. 4(a) and 4(b).

An important issue is the behavior of $\tau_{\rm int}^{(2)}$ at high bias fields $\xi_0 \gg 1$. As follows from the above-presented considerations, in the hard-dipole model one has $\tau_{\rm int}^{(2)} \propto 1/\xi_0$. For the case of particles with finite magnetic anisotropy we assume that at sufficiently high bias fields ($\xi_0 > 2\sigma$) magnetic metastability is suppressed. Due to that the renormed time $\tilde{\tau}_D$ does not differ from the real one τ_D and the behavior of the system is close to that in the "kinetic cutoff" limit. This grants validity to the effective-field result (57). Expanding it to the first order in $1/\xi_0$, one gets

$$\left.\frac{\tau_{\rm int}^{(2)}(\xi_0,\sigma)}{\tau_B}\right|_{\tilde{\varepsilon}=0} = g_1(\sigma) + \frac{g_2(\sigma)}{\xi_0}, \tag{62}$$

where the coefficients g are expressed as

$$g_1(\sigma) = \frac{2}{3}\,\frac{7 + 5S_2(\sigma) - 12S_4(\sigma)}{14 + 5S_2(\sigma) + 16S_4(\sigma)}, \tag{63}$$

$$g_2(\sigma) = \frac{70}{3}\,\frac{-3S_2(\sigma) + 28S_2(\sigma)S_4(\sigma) + 80S_4(\sigma)}{[14 + 5S_2(\sigma) + 16S_4(\sigma)]^2},$$

and have the following limiting behavior:

$$g_1(\sigma) = \begin{cases} \dfrac{1}{3} + \dfrac{1}{63}\sigma - \dfrac{5}{441}\sigma^2 + \cdots & \text{for } \sigma \ll 1, \\ \dfrac{1}{\sigma} + \dfrac{1}{\sigma^2} - \dfrac{1}{\sigma^3} + \cdots & \text{for } \sigma \gg 1, \end{cases} \tag{64}$$

$$g_2(\sigma) = \begin{cases} -\dfrac{1}{21}\sigma + \dfrac{160}{1323}\sigma^2 + \cdots & \text{for } \sigma \ll 1, \\ 2 - \dfrac{1}{\sigma} - 12\sigma^2 - \dfrac{23}{\sigma^3} + \cdots & \text{for } \sigma \gg 1. \end{cases}$$

Accordingly, the behavior of the integral relaxation time described in the leading order is

$$\left.\frac{\tau_{\rm int}^{(2)}}{\tau_B}\right|_{\tilde{\varepsilon}=0} = \begin{cases} \dfrac{1}{3} - \dfrac{1}{21}\,\dfrac{\sigma}{\xi_0} & \text{for } \sigma \ll 1, \\ \dfrac{1}{\sigma} + \dfrac{2}{\xi_0} & \text{for } \sigma \gg 1. \end{cases} \tag{65}$$

Thus we conclude that the birefringence relaxation processes are quite different for the particles with low and high magnetic anisotropy. For the former, $\tau_{\rm int}^{(2)}$ is about $\tau_B/3$ and prac-

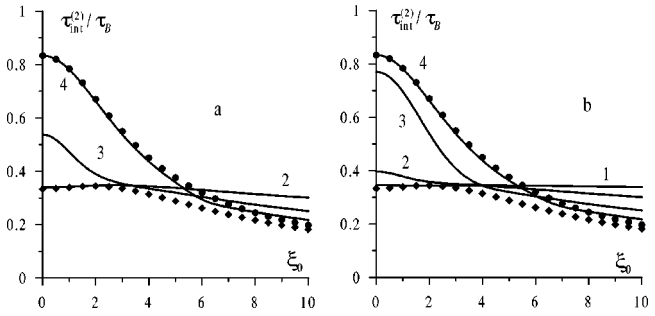

FIG. 4. Modified integral relaxation time of orientation as a function of the dimensionless bias field ξ_0. Solid curves are calculated for $\varepsilon = 10^{-3}$ (a) and $\varepsilon = 10^{-2}$ (b) at the anisotropy parameter $\sigma = 2$ (1), 5 (2), 10 (3), and 20 (4). Lines of markers show the limiting contours $\sigma = \infty$: full circles correspond to the hard dipole case described by Eq. (32) while diamonds mark $\tau_{\rm int}^{(2)}$ in the "kinetic cutoff" limit, i.e., $\varepsilon \equiv 0$.

tically independent of the bias field. For high σ the relaxation time in general obeys the hyperbolic law $2/\xi_0$ well known for magnetically hard ($\sigma=\infty$) particles. However, due to the presence of a term independent of ξ_0, the limit of the relaxation time at $\xi_0\to\infty$ is always finite and not zero as it is in the case of hard dipoles.

We remark that the found existence of a finite limit of $\tau_{\rm int}^{(2)}$ at $\xi_0\to\infty$ has an important consequence with respect to the experiment interpretation. Normally, when anticipating power laws, the measurement data are plotted in double logarithmic coordinates. In the case of a hard dipole this gives a straight line, irrespective of whether magnetic or orientational susceptibility is studied. If, however, the dipole has a finite rigidity so that the relaxation time at high bias fields is described by the second line of Eq. (65), the double logarithmic representation has to be used with caution. Indeed, as Eq. (65) shows, a plot $\ln(\tau_{\rm int}^{(2)})$ *may be close to a straight line only for* $\xi_0<2\sigma$. But this range might be empty if σ is not large enough since Eq. (65) is the *asymptotic* form valid for $\xi_0\gg 1$. In the range of its unquestionable validity, i.e., where both $\xi_0,\ \sigma\gg 1$, the function $\tau_{\rm int}^{(2)}(\xi_0)$ plotted in double logarithmic coordinates gives a line with a slope that gradually changes from unity to zero as the term $\propto 1/\xi_0$ diminishes in comparison to the constant one. These considerations equally apply if one changes the roles of ξ_0 and σ, and plots the relaxation time as a function of σ at a given ξ_0.

In the linear response theory the relaxation time does not depend on the magnitude of the probing field. If the system is single mode, then the relaxation time derived for a transient process can be equally used to write the stationary solution under the action of an ac probing field. For a system with multimode response the independence from the probing field amplitude, of course, holds but the reference (integral) times might differ depending on the way of probing, pulse or ac. To study a MF in a crossed-field situation where the probing field is alternating and not pulse, one has to solve the equation

$$\frac{d}{dt}\ Q_i+\Gamma_{il}\ N_{lk}^{-1}Q_k=\Gamma_{i1}\xi(t), \tag{66}$$

cf. Eq. (53). To obtain a stationary solution, it suffices to take $\xi=\xi^{(0)}\exp(-i\omega t)$, substitute it in Eq. (66), and resolve the resulting matrix set. This yields a one-column matrix with complex elements Q_1 and Q_2. Setting the amplitude $\xi^{(0)}$ of the probing field equal to unity (which is here equivalent to differentiation) we get the respective dynamic susceptibilities. In particular, Q_2 is the complex susceptibility of the orientation order parameter to an external magnetic field. With regard to the geometry of the magneto-optical experiment in crossed fields [6], one finds that the theoretical quantity proportional to the measured transmitted light intensity is the square of the orientational order parameter. Accordingly, under stationary oscillations, the effective dynamic susceptibility that is measured is the square of the susceptibility Q_2.

V. DISCUSSION OF THE RESULTS

In Ref. [6] the dynamics of birefringence is discussed in terms of some characteristic time derived from the experimental data in the following way. The intensity $I_{2\omega}$ of the light transmitted by the sample under the joint action of crossed dc and ac fields is plotted as a function of frequency and the frequency ω_* is found, at which $I_{2\omega}(\omega_*)=\frac{1}{2}I_{2\omega}(0)$. The quantity inverse to ω_* is taken as a reference response time and is denoted as $\tau_{\rm exp}$.

To apply the developed model to the experiment [6], we construct a direct theoretical analog of $\tau_{\rm exp}$. For that we take the solution of Eq. (66), impose on it the condition $Q_2^2(\omega_*)=\frac{1}{2}Q_2^2(0)$, and obtain ω_* as the function of ξ_0 and σ by resolving the pertinent transcendental equation. The inverse of the found ω_* is the sought for reference time that we denote as $\tau_{1/2}$. A set of curves presenting the obtained function is given in Fig. 5 together with dash-dotted straight lines rendering the power law $1/\xi_0$ inherent to a hard dipole and asymptotes (dashed lines) at large ξ_0 obtained numerically from expansion of solutions of Eq. (66) at $\xi_0\gg 1$. As is intuitively expectable, $\tau_{1/2}$ is close to the integral relaxation time $\tau_{\rm int}^{(2)}$ defined in Sec. IV C. A direct comparison presented in Fig. 6 supports this conclusion; the occurring similarity transforms into coincidence in the high-field end.

In Ref. [6] in the crossed-field geometry two sets of magnetic fluid samples were investigated. Namely, there were five samples containing cobalt ferrite nanoparticles and two samples whose magnetic phase consisted of maghemite nanoparticles. In the cobalt ferrite grains the magnetic anisotropy is of the volumetric origin and rather strong. Therefore, their behavior under field should resemble that of hard dipoles. On the contrary, for maghemite grains, where the anisotropy is known to be of the surface origin, and much weaker, the response is expected to resemble that of soft dipoles. The particle size distributions were determined in Ref. [6] from measurements of the equilibrium magnetization and were found to be close to log-normal ones described by the size parameter d_0 and dimensionless width s. The magnetization of the cobalt ferrite is taken to be $I=350$ kA/m and that for maghemite particles $I=320$ kA/m. The volume energy density of uniaxial magnetic anisotropy for the cobalt ferrite is $K_V=500$ kJ/m^3, the respective surface energy density for maghemite is $K_S=2.8\times10^{-5}$ J/m^2. Using these numerical values, one can estimate the anisotropy parameters σ. We do that assuming that the particle magnetic volume is $V_m=(\pi/6)\overline{d^3}$ and the particle surface area that matters for estimation of the anisotropy of the surface origin is $S_m=\pi\overline{d^2}$, where the overline means averaging over the corresponding log-normal histogram. The initial histogram data and the results of our estimations are given in Table I [20]. As in Ref. [6], we mark the cobalt ferrite samples by "*C*" and the maghemite ones by "*M*."

In the qualitative aspect we remark a full agreement between the shapes of dispersion curves derived from the finite-anisotropy model by solving Eq. (66) and the experi-

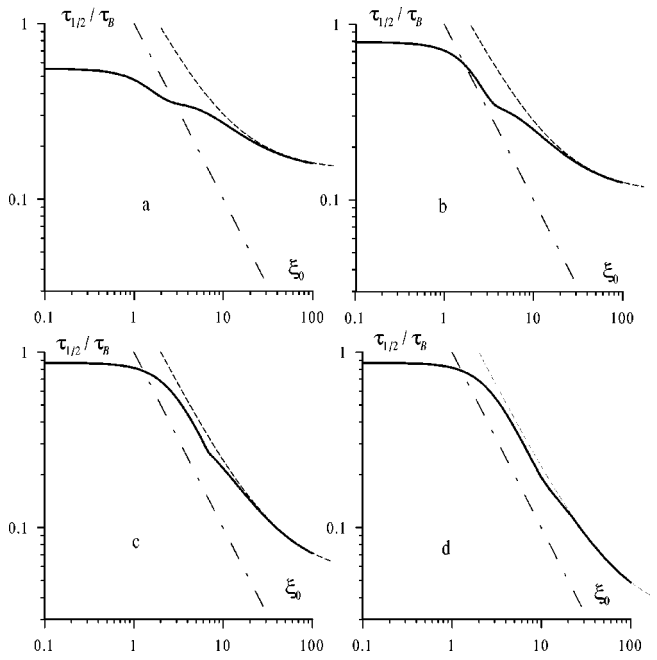

FIG. 5. Bias-field dependencies of the theoretical analog $\tau_{1/2}$ of the reference relaxation time $\tau_{\exp}$. The anisotropy parameter is $\sigma=7.5$ (a), 10 (b), 20 (c), and 35 (d); for all the curves $\varepsilon=10^{-2}$. Dashed-dotted lines indicate a simple power law $1/\xi_0$; dashed lines show the asymptotes (large ξ_0) obtained numerically from the solutions of Eq. (66).

mental ones given in Ref. [6]. Presenting those dynamic susceptibilities in the form of Argand diagrams ($\mathrm{Im}\,Q_2^2$ plotted against $\mathrm{Re}\,Q_2^2$) one becomes aware of their splitting with respect to both ξ_0 and σ. Qualitatively, such splitting is clearly visible in the experimental Argand diagrams of Ref. [6] but was never accounted for. In our theory, splitting is a natural consequence of the finiteness of the anisotropy of the particles. Depending on whether $\tilde{\tau}_D$ is greater or smaller than τ_B, the Argand loops might either ''deflate'' or ''inflate'' with respect to the reference (single-time) contour. The crossover of the relaxation regimes that takes place at $\tilde{\tau}_D \approx \tau_B$ provokes, as its consequence, a peculiar reentrant behavior (''breath'') of the Argand loops. However, the analysis of this interesting effect is beyond the scope of the present work, and will be given elsewhere.

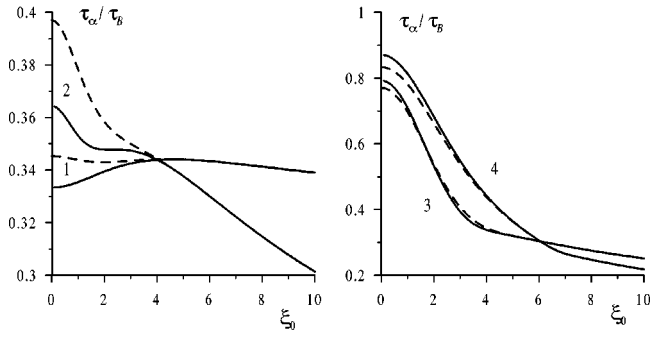

FIG. 6. Comparison of the bias-field dependencies of the integral relaxation time $\tau_{\mathrm{int}}^{(2)}$ (dashed lines) and the reference relaxation time $\tau_{1/2}$ (solid lines) for $\sigma=2$ (1), 5 (2), 10 (3), 20 (4); for all the curves $\varepsilon=10^{-2}$.

TABLE I. Size distribution and anisotropy parameters of the samples.

Sample	d_0 (nm)	s	σ	ξ_0/H_0 (m/kA)
C_1	12.7	0.35	225	0.197
C_2	9.0	0.20	55	0.050
C_3	8.7	0.16	47	0.043
C_4	7.0	0.20	26	0.022
M_1	9.4	0.10	2.0	0.043
M_2	9.2	0.15	2.0	0.043

With regard to the quantitative comparison, from Table I we conclude that the cobalt ferrite sample C_1 with its $\sigma>200$ may be well treated in the hard-dipole approximation, while for sample C_3 that has $\sigma\sim 50$ some corrections may be ''visible.'' Using this scheme, for C_1 we calculate the function $\tau_{1/2}(\xi_0)$ for $\sigma=\infty$ (see Fig. 1) while for C_3 calculation is done according to the full procedure for $\tau_{1/2}$. Considering τ_B as an adjustable parameter, we evaluate it on the ''chi-by-the-eye'' basis and plot the results in Fig. 7(a). The achieved agreement between theory and experiment is satisfactory; the absolute values of the Brownian relaxation times that we have got in our interpretation are $\tau_B=4.1$ ms for C_1 and $\tau_B=0.43$ ms for C_3. Figure 7(b) shows the same adjustment for samples C_2 and C_4, where we get $\tau_B=1.64$ ms and $\tau_B=0.54$ ms, respectively.

In Fig. 8 the data on the cobalt ferrite samples C_1 to C_4 are presented in double logarithmic coordinates. It is instructive to see, to what extent the obtained curves look like straight lines (hard-dipole model) and to what extent they deviate at lower fields (below the cutoff introduced in Ref. [6]).

In Ref. [6], on the basis of qualitative considerations, the idea was inferred that for magnetically soft nanoparticles, as

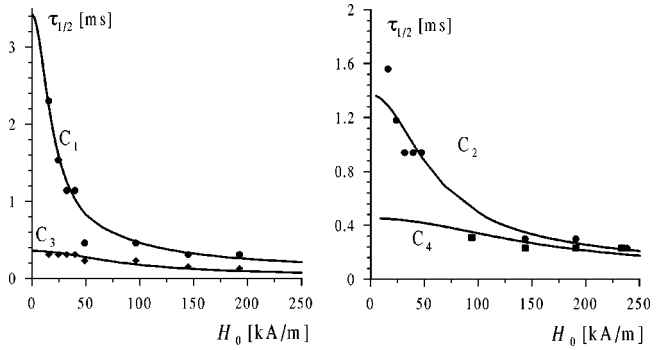

FIG. 7. Comparison of the bias-field dependencies of the reference relaxation time $\tau_{1/2}$ with the experimental measurements on the cobalt ferrite samples; for all the curves $\varepsilon=2\times10^{-4}$. (a) samples C_1 (full circles) and C_3 (diamonds); the estimated values of the rotary diffusion time are $\tau_B=4.1$ ms (C_1) and $\tau_B=0.43$ ms (C_3). (b) Samples C_2 (full circles) and C_4 (squares); the estimated values are $\tau_B=1.64$ ms (C_2) and $\tau_B=0.54$ ms (C_4).

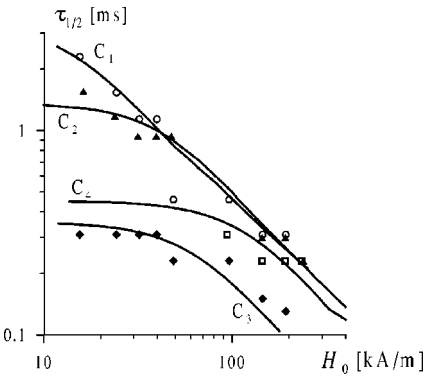

FIG. 8. Comparison of the theoretical bias-field dependencies of the reference relaxation time $\tau_{1/2}$ (solid lines marked with the sample identifiers) with the experimental measurements on the cobalt ferrite samples C_1 (empty circles), C_2 (triangles), C_3 (diamonds), and C_4 (squares); for all the curves $\varepsilon=2\times10^{-4}$.

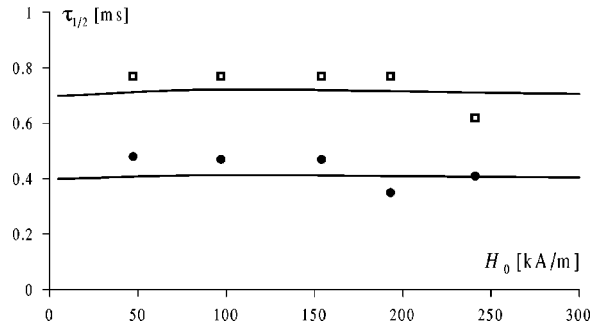

FIG. 9. Comparison of the theoretical bias-field dependencies of the reference time $\tau_{1/2}$ with the experimental $\tau_{\rm exp}$ for the maghemite samples M_1 (circles) and M_2 (squares). The lines correspond to the anisotropy parameter $\sigma=2$ (see Table I) and $\varepsilon=2\times10^{-5}$. The reference rotary diffusion times are $\tau_B=1.2$ ms (M_1) and $\tau_B=2.1$ ms (M_2).

soon as the external field H_0 exceeds the internal one H_a, the relaxation time $\tau_{\rm exp}$ in a MF becomes independent of H_0. The maghemite ferrofluid samples M_1 and M_2 are good candidates for the test: as Table I shows, they both have $\sigma\sim1$. Since the samples under consideration are the ferrofluids based on glycerine whose viscosity is $\eta\sim10$ Ps, the estimate for the ratio $\tau_D/\tau_B=\varepsilon$ gives 10^{-4}–10^{-5}. With $\sigma\sim1$ this means that both MF samples are very close to the ''kinetic cutoff'' limit. Under these conditions the theoretical relaxation time $\tau_{1/2}$ is but weakly dependent on the bias field ξ_0 that agrees well with the weak dependence of $\tau_{\rm exp}$ on H_0 experimentally found in Ref. [6] and justifies the hypothesis proposed therein. In Fig. 9 the theoretical curves obtained with Eq. (57) at $\sigma=2$ are compared with the data of Ref. [6] on the maghemite samples. The numerical values of the rotary diffusion time that we get from the adjustment are $\tau_B=1.2$ ms for sample M_1 and $\tau_B=2.2$ ms for sample M_2. According to the present model $\tau_{\rm exp}$ should be virtually independent of H_0 in the low-field range as well.

VI. CONCLUSIONS

Theory for dynamic birefringence in a magnetic fluid subjected to a joint action of crossed bias (constant) and probing (pulse or ac) fields is developed. Under the considered field configuration the induced birefringence is linear with respect to the probing field, so that the linear response approximation is possible. The suspended nanoparticles are assumed to possess finite magnetic anisotropy of the easy axis type, whose direction coincides with the major geometry axis. To allow for the finiteness of the anisotropy, the general Fokker-Planck equation that takes into account both internal magnetic and external mechanical degrees of freedom of the particles is used.

The particle orientation dynamics, which is in general a multimode process, is described in terms of the integral relaxation times for the two lowest statistical moments of the distribution function, namely, the magnetization and the orientation order parameter. The results for the limiting cases of weak and strong bias fields are given in an analytical form. For the intermediate case an interpolation expression for the integral relaxation time of birefringence is proposed and proven to have a physically reasonable overall behavior.

The developed description is applied to the experimental data on crossed-field birefringence of MF samples with nanoparticles of two types: magnetically hard (cobalt ferrite) and magnetically soft (maghemite). Observations evidence that the differences in the particle properties are essentially reflected in the dynamics of macroscopic birefringence of the samples. The proposed theory appears to be in full qualitative agreement with all the experimental data available.

ACKNOWLEDGMENTS

Y.L.R. and V.I.S. acknowledge partial support by Award No. PE-009-0 of the U.S. Civilian Research & Development Foundation for the Independent States of the Former Soviet Union (CRDF) and by Grant No. 02-02-17221 from the Russian Foundation for Basic Research (RFBR).

APPENDIX

The general matrix equation of the problem that determines the amplitudes $Q_{l\,l'}^{mm'}$ is obtained by substitution of the spherical harmonic expansion (12) into the Fokker-Planck equation (4). After that the equation is multiplied from the left by $X_l^m(\boldsymbol{e},\boldsymbol{n})X_{l'}^{m'}(\boldsymbol{n},\boldsymbol{h})$, and, finally, integrated with respect to both $\boldsymbol{e}$ and $\boldsymbol{n}$. The result is

$$\frac{d}{dt}Q_{l,l'}^{m,m'}+\frac{1}{2\tau_D}\,l(l+1)Q_{l,l'}^{m,m'}+\frac{1}{2\tau_B}\,l'(l'+1)Q_{l,l'}^{m,m'}-\frac{\sigma}{\tau_D}\left[\frac{(l+1)(l+m-1)(l+m)}{(2l-1)(2l+1)}\,Q_{l-2,l'}^{m,m'}+\frac{l(l+1)-3m^2}{(2l-1)(2l+3)}\,Q_{l,l'}^{m,m'}\right.$$

$$\left.-\frac{l(l-m+2)(l-m+1)}{(2l+1)(2l+3)}\,Q_{l+2,l'}^{m,m'}\right]-\frac{\xi}{2\tau_D(2l+1)(2l'+1)}\Big\{(l+1)(l+m)[(l'-m'+1)Q_{l-1,l'+1}^{m,m'}+(l'$$

$$+m')Q_{l-1,l'-1}^{m,m'}]-l(l-m+1)[(l'-m'+1)Q_{l+1,l'+1}^{m,m'}+(l'+m')Q_{l+1,l'-1}^{m,m'}]+\frac{1}{2}\,(l+1)(l+m-1)(l+m)[(l'+m'$$

$$-1)(l'+m')Q_{l-1,l'-1}^{m-1,m'-1}-(l'-m'+1)(l'-m'+2)Q_{l-1,l'+1}^{m-1,m'-1}]+\frac{1}{2}\,l(l-m+2)(l-m+1)[(l'+m'-1)(l'$$

$$+m')Q_{l+1,l'-1}^{m-1,m'-1}-(l'-m'+1)(l'-m'+2)Q_{l+1,l'+1}^{m-1,m'-1}]-\frac{1}{2}\,(l+1)(Q_{l-1,l'+1}^{m+1,m'+1}-Q_{l-1,l'-1}^{m+1,m'+1})-\frac{1}{2}\,l(Q_{l+1,l'+1}^{m+1,m'+1}$$

$$-Q_{l+1,l'-1}^{m+1,m'+1})\Big\}-\frac{\xi}{2\tau_B(2l+1)(2l'+1)}\Big\{(l'+1)(l'+m')[(l-m+1)Q_{l+1,l'-1}^{m,m'}+(l+m)Q_{l-1,l'-1}^{m,m'}]-l'(l'-m'+1)$$

$$\times[(l-m+1)Q_{l+1,l'+1}^{m,m'}+(l+m)Q_{l-1,l'+1}^{m,m'}]+\frac{1}{2}\,(l'+1)(l'+m'-1)(l'+m')[(l+m-1)(l+m)Q_{l-1,l'-1}^{m-1,m'-1}-(l-m$$

$$+1)(l-m+2)Q_{l+1,l'-1}^{m-1,m'-1}]+\frac{1}{2}\,l'(l'-m'+2)(l'-m'+1)[(l+m-1)(l+m)Q_{l-1,l'+1}^{m-1,m'-1}-(l-m+1)(l-m$$

$$+2)Q_{l+1,l'+1}^{m-1,m'-1}]-\frac{1}{2}\,(l'+1)(Q_{l+1,l'-1}^{m+1,m'+1}-Q_{l-1,l'-1}^{m+1,m'+1})-\frac{1}{2}\,l'(Q_{l+1,l'+1}^{m+1,m'+1}-Q_{l-1,l'+1}^{m+1,m'+1})\Big\}=0. \tag{A1}$$

[1] J.-C. Bacri and R. Perzynski, in *Complex Fluids*, edited by L. Garrido (Springer, New York, 1993), p. 85.

[2] Yu.L. Raikher and V.I. Stepanov, Europhys. Lett. **32**, 589 (1995).

[3] Yu.N. Skibin, V.V. Chekanov, and Yu.L. Raikher, Zh. Éksp. Teor. Fiz. **72**, 949 (1977) [Sov. Phys. JETP **45**, 496 (1977)].

[4] Yu.L. Raikher and Yu.N. Skibin, Dok. Akad. Nauk (SSSR) **302**, 1088 (1988) [Sov. Phys. Dokl. **302**, 746 (1988)].

[5] Yu.L. Raikher and P.C. Scholten, J. Magn. Magn. Mater. **74**, 275 (1988).

[6] E. Hasmonay, E. Dubois, S. Neveu, J.-C. Bacri, and R. Perzynski, Eur. Phys. J. B **21**, 19 (2001).

[7] Yu.L. Raikher and M.I. Shliomis, Adv. Chem. Phys. **87**, 595 (1994).

[8] V.I. Stepanov and M.I. Shliomis, Izv. Akad. Nauk SSSR, Ser. Fiz. **55**, 1 (1991) [Bull. Acad. Sci. USSR, Phys. Ser. (Engl. Transl.) **55**, 1 (1991)].

[9] M.I. Shliomis and V.I. Stepanov, J. Magn. Magn. Mater. **122**, 176 (1993); **122**, 196 (1993).

[10] M.I. Shliomis and V.I. Stepanov, Adv. Chem. Phys. **87**, 1 (1994).

[11] W.F. Brown, Jr., Phys. Rev. **130**, 1677 (1963).

[12] R. Ullman, J. Chem. Phys. **56**, 1869 (1972).

[13] M.A. Martsenyuk, Yu.L. Raikher, and M.I. Shliomis, Zh. Éksp. Teor. Fiz. **65**, 834 (1977) [Sov. Phys. JETP **38**, 413 (1974)].

[14] H. Risken, *The Fokker-Planck Equation* (Springer, Berlin, 1984).

[15] W.T. Coffey, P.J. Cregg, D.S.F. Crothers, J.T. Waldron, and A.W. Weakstead, J. Magn. Magn. Mater. **131**, L103 (1994).

[16] Yu.L. Raikher, V.I. Stepanov, A.N. Grigorenko, and P.I. Nikitin, Phys. Rev. E **56**, 6400 (1997).

[17] A. Aharoni, Phys. Rev. **177**, 799 (1969).

[18] E. Blums, A. Cebers, and M. Maiorov, *Magnetic Fluids* (de Gruyter, Berlin, 1997).

[19] M.C. Miguel and J.M. Rubí, Phys. Rev. E **51**, 2190 (1995).

[20] Note that in these estimations the average volume is taken as proportional to $\overline{d^3}$ and not to d_{mp}^3 as in Ref. [6]. We surmise that it is more realistic since d_{mp}, being the most probable diameter, does not have any other meaning. The numerical estimations for σ (and ξ_0) that we get are considerably greater that those given in Ref. [6] due to two reasons: (1) a different way of definition of the average volume and (2) an error in Ref. [6], due to which the value of K_V really used there was 2.5 times smaller than the one announced in the text.